INTERACTION BETWEEN $10^{11} - 10^{12}$ ev PARTICLES AND IRON NUCLEI

N. L. GRIGOROV, V. S. MURZIN, and I. D. RAPOPORT

Institute of Nuclear Physics, Moscow State University

Submitted to JETP editor November 4, 1958

J. Exptl. Theoret. Phys. (U.S.S.R.) **36**, 1068-1079 (April, 1959)

The following characteristics of the elementary interaction between $10^{11} - 10^{12}$ ev cosmic ray particles and iron nuclei were studied at elevation 3860 m by means of apparatus which determined the "primary" particle energy: a) the inelastic cross section, b) the degree of inelasticity of the interaction, c) the distribution function of energy transferred to π^0 mesons and certain other properties.

1. INTRODUCTION

AFTER the fundamental work of Powell and his coworkers[1] showed that interactions between cosmic rays and atomic nuclei produce pions, detailed investigations of interactions with high-energy cosmic rays were conducted to determine the meson-producing mechanism, particularly the energy dependence of the processes involved and the nature of the "primary" particles. Some experiments which aimed to select primary particles of specified energies (mainly in the stratosphere) made use of the geomagnetic effect, while other experiments employed cloud chambers placed in a magnetic field. Since the earth's magnetic field has practically no effect on particles with a few tens of billions of electron volts the use of the geomagnetic effect to select primary particles is practically confined to energies below about 20×10^9 ev. A cloud chamber in a magnetic field is only slightly more advantageous. Thus the study of interactions with particles possessing 10^{11} to 10^{12} ev and above requires new methods of measuring primary particle energies.

During recent years extensive use has been made of nuclear emulsions to determine primary particle energies from the emission angles of secondary particles created in nuclear reactions with primary particles. However the degree of reliability of this method has still not been determined and experimental verification of the results requires some independent means of measuring primary particle energies.

In a search for such means we have made use of the fact that strong interactions between nuclei and high-energy nuclear-active particles (the N component) are followed by the absorption of the primary particle and of all its descendants in relatively thin layers of matter of the order 1000 g/cm^2. The energy of a primary particle is ultimately expended for the ionization of atoms in the medium where absorption occurs. Therefore when we measure the total number of ion pairs produced in a layer of the order 1000 g/cm^2 through the absorption of a single primary particle, knowledge of the energy ϵ required to produce a single ion pair makes it easy to determine the energy E_0 of a particle entering the absorber:

$$E_0 = \varepsilon \int_0^{x_0} I(x)\,dx, \qquad (1)$$

where $I(x)\,dx$ is the ionization in a layer of thickness dx g/cm^2 at depth x g/cm^2 and x_0 is the total thickness of the absorber.

This technique for determining energies resembles calorimetric measurements and the apparatus that we have accordingly designed for the purpose[2] will be called an "ionization calorimeter." In practice ionization is not measured along a continuous line through the absorber but at discrete levels $x_1, x_2, \ldots, x_n$ under layers of finite thickness. From the ionization $I(x_i)$ measured under layers of thickness x_i we can plot a smooth $I(x)$ curve to be used in (1) for the determination of E_0. It is evident that the accuracy of E_0 will increase with the number of layers. In order to reduce the minimum number of layers in an ionization calorimeter required for satisfactory accuracy of E_0 it is desirable to use an absorbing material in which the mean free path for nuclear interaction and the electron-photon cascade range are of the same order. The thickness of layers between adjacent ionization detectors should be of the order 6 or 8 cascade units.

Special mention must be made of the fact that as the primary particle energy E_0 increases it is determined more accurately by an ionization calorimeter. This results from the fact that with increasing E_0 a relatively smaller fraction of the energy is transferred to strongly ionizing products of nuclear disintegrations, whose energy is measured with small efficiency by our apparatus. We estimate the accuracy of E_0 at about 30% in the vicinity of 10^{11} ev.

It is evident that the ionization calorimeter, which is of relatively simple construction, can easily be combined with other techniques for observing particles. For example, in a cloud chamber placed above an ionization calorimeter we can observe the elementary interaction of a particle of known energy and study various properties of this interaction (dependence on the atomic weight of the nucleus and primary particle energy) at $\sim 10^{11}$ or 10^{12} ev. In a magnetic field the cloud chamber also permits analysis of secondary particles.

At the time when we raised an ionization calorimeter to an elevation of 3860 m an auxiliary large cloud chamber was still not ready. Therefore our published data pertain only to processes which can be studied with only a single ionization calorimeter. It will be seen that an investigation of the dynamics of electron-nuclear cascades in dense matter (by using a large number of detectors which register ionization independently of each other) not only provides a reliable primary particle energy measurement in each individual instance but also enables us to investigate such properties of an elementary event as a) the degree of elasticity of the interaction between the primary particle and absorber nuclei in the ionization calorimeter, b) the degree of inelasticity of secondary-particle interactions, c) the secondary-particle energy spectrum, d) the distribution of the energy fraction which is transferred to π^0 mesons in a primary-particle interaction, e) the cross section for inelastic interactions between primary particles and absorber nuclei and its dependence on the primary particle energy.

2. APPARATUS

The ionization calorimeter used in our experiments was a large assembly of seven layers of iron alternating with six rows of pulse ionization chambers (Fig. 1, I-VI). A more detailed description has been given in reference 2. A single ionization detector was formed by connecting three chambers in parallel. Each detector was connected to an amplifier with a dynamic range of 800, and was sensitive enough for the reliable

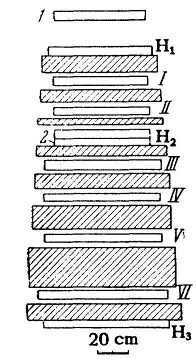

FIG. 1. Schematic cross section of setup. I – VI) rows of ionization chambers; 1, 2) rows of telescopic counters; $H_1 - H_3$) boxes with hodoscopic counters.

registration of 5 to 10 relativistic particles passing through it simultaneously. Signals from the amplifiers were fed to oscilloscopes mounted in a separate assembly, the construction and operation of which have been described in reference 3. Also, signals from the amplifiers were fed to a sum circuit which combined all pulses from a single row of ionization chambers. Pulses were recorded by photographing the oscilloscope screens at the instant when all oscilloscope beams were triggered by a master signal. Altogether 105 ionization chambers were used, forming 35 independent detectors. The total thickness of iron between rows of ionization chambers was 650 g/cm^2 and the total thickness of the iron assembly was 750 g/cm^2.

In addition to the ionization chambers the apparatus included three boxes of gas-discharge tubes which served as hodoscopic counters (H_1, H_2, H_3). Each box contained two rows of counters, the axes of counters in one row being perpendicular to the axes in the other row. The hodoscopic counters were glass tubes 70 to 90 cm long, 2 cm in diameter with an Aquadag anode and filament of 100 μ diameter. These counters were filled with pure argon to ~ 100 mm Hg and were subjected to a voltage pulse of 2×10^{-5} sec duration at the instant when coincident discharges occurred in the two boxes of telescopic counters (1 and 2). The hodoscopic counters were connected to MTX-90 neon bulbs, which were photographed independently.

The hodoscopic counters enabled us to determine the air-shower accompaniment of high-energy nuclear-active particles (box H_1), and the direction of the electron-nuclear cascade core within the ionization calorimeter absorbing material in a plane parallel to the chamber axes (boxes H_2 and H_3).

Two rows of telescopic counters (1 and 2) served mainly to produce a master signal with the minimum delay required for control of the hodoscopic counters (when the pulse to the gas-discharge tubes was delayed by not more than 2×10^{-6} sec they exhibited 94% efficiency in the recording of charged particles). The neon bulbs of the hodoscope were photographed only at the instants when a high-energy particle struck the ionization calorimeter; the pulse which triggered the oscilloscope beams simultaneously applied a voltage to the anodes of the neon bulbs, in the hodoscope.

The master signal was produced as follows. All simultaneous ionization pulses from each row of ionization chambers were summed, as has already been mentioned. The resultant signal was fed to a selector, which was triggered when a few rows of ionization chambers simultaneously produced resultant signals above a predetermined threshold V_{thr}. A master pulse resulted from simultaneous triggering of the selector and discharges in both rows of telescopic counters. Our data were obtained through the simultaneous triggering of any two or more rows of chambers, in which case V_{thr} was equivalent to 250 relativistic particles traversing the mean chords of the chambers.

The requirement of simultaneous ionization > V_{thr} in two rows of chambers considerably reduced the number of events resulting from low-energy nuclear disintegrations, and a sufficiently high value of V_{thr} insured the registration of nuclear-active particles with energies of about 10^{11} ev and higher.

3. TREATMENT OF RESULTS

Pulses from the ionization chambers were fed to a multi-channel oscilloscope and were photographed on motion picture film which also recorded the electronic calibration of all amplifying channels. The first step in the treatment of these data was the measurement of ionization-chamber pulse heights and the determination of the ionization produced in each chamber. The ionization was converted to the number of relativistic particles passing through the chambers whenever required. The results were used to plot a diagram showing the distribution of ionization along a row of chambers and the absorber depth for each separate case. Typical diagrams are shown in Fig. 2. These diagrams were used to determine the angle of incidence of the primary particles.

A picture of the triggered hodoscopic counters was obtained at the same time. This could be done in two projections to determine the shower inclination in a projection along the ionization chamber axes. These diagrams helped to determine whether a significant fraction of shower energy passed through the side walls of the ionization calorimeter.

4. RESULTS

The majority of events registered by our selection scheme were induced by nuclear-active particles from the atmosphere, but our apparatus also efficiently registered electrons and photons (the latter accompanied by charged particles) as well as air showers and muon bursts.

In the present paper we analyze 110 instances in which more than 250 relativistic particles passed through any two rows of ionization chambers. A division was made into a few groups depending on the character of the observed events. The ionization was sometimes distributed more or less uniformly along the first two or more rows, falling off rapidly with depth; these instances were interpreted as air showers, of which 17 were recorded. In a number of instances the ionization in the chambers revealed a distinct core, with the ionization versus depth curve in good agreement with electromagnetic cascade theory.[4] When such an event took place at the edge of our absorber (shown by large ionization in the first row) there was strong reason to attribute it to an electron or

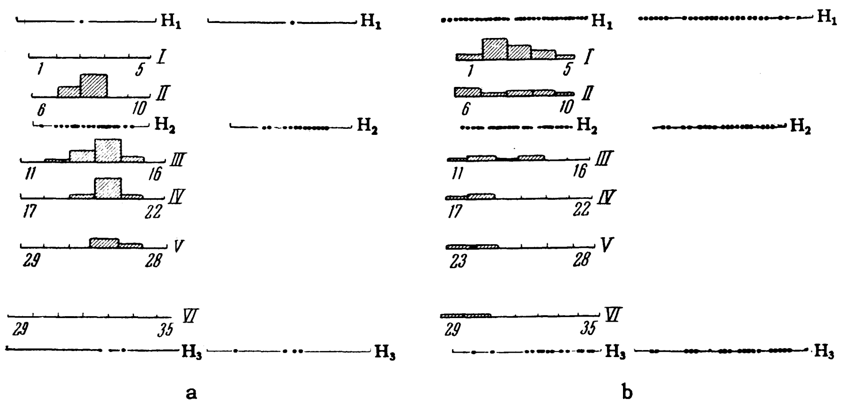

FIG. 2. Distribution of ionization in the ionization calorimeter for a – incident nuclear-active particle, b – air shower. The positions of rows of ionization chambers are indicated by the numerals I – VI. The numerals 1 – 35 denote individual ionization detectors. The heights of the rectangles represent the ionization recorded by these detectors, in relative units. The dots show the arrangement of triggered hodoscopic counters.

photon. A shower originating within the absorber suggests production through muon bremsstrahlung (in the case of two showers).

It should be noted that whenever the interaction of a nuclear-active particle with a nucleus resulted in the entire energy being transferred to π^0 mesons the event was attributed to an electron or a muon depending on the point of origin. This might somewhat reduce the mean energy losses that we determined for pion production. All other observed events showed a distinct core (Fig. 2a) and varying shapes of the ionization versus depth curves, all of which were considerably broader than electron-photon cascade curves and often showed secondary maxima within the absorber or slow falling-off of ionization with depth.

These curves are evidence of secondary interactions in the apparatus and of additional energy transfer to the electron-photon component under considerable depths of matter. We classified such events as nuclear interactions with primary particles and selected them for analysis.

In most instances a comparison of ionization hodoscope and counter data enabled us to determine whether the shower core passed through the side of the apparatus; such showers were excluded from the data. Thirty-two showers were selected with cores within the solid angle of the ionization hodoscope (see the table). These were distributed as follows: Four showers possessed a "structure," with two cores separated by 25 to 40 cm. In the three cases when the energy of both particles could be determined the energy ratios were 1 : 2, 1 : 5 and 2 : 3. Ten nuclear-active particles had energy $\gtrsim 10^{12}$ ev and 22 were between 10^{11} and 10^{12} ev.

No.	Particle energy, 10^{11} ev	Angle to vertical, deg	Point of first interaction, g/cm²	Number of particles in first maximum	Number of particles in second maximum	Number of particles accompanying electron*	Remarks
1	10.0	23	<50	2300	>1200	$\geqslant 11$	
2	>1.0	<10	~ 0	270	—	$\geqslant 15$	Structured shower; a single particle is analysed
3	1.5	19	~ 0	430	—	11	
4	1.4	?	~ 0	580	330	6	
5	1.7	$\geqslant 17$	~ 0	~ 300	420	$\geqslant 20$	
6	4.8	22	50	1550	—	$\geqslant 25$	Energy of accompanying particles** $\sim 4.5 \times 10^{10}$ ev
7	4.0	15	<50	40	230	3	
8	7.8	14	<50	1470	1000	8	
9	4.0	~ 15	30	1250	—	—	
10	16.0	10	50	3120	~ 1500	11	
11	3.0	23	100—200	490	~ 300	~ 20	Energy of accompanying particles** $\sim 9 \times 10^{10}$ ev
12	2.5	20	50	340	440	—	
13	3.0	<10	100	880	—	—	
14	0.7	24	~ 0	360	—	~ 20	Structured shower; a third maximum exists with $n_3 = 50$
	0.5	24	100	220	275		
15	9.7	20	300	1550	—	—	
16	3.5	22	<50	200	1500	—	
17	3.5	0	~ 0	3200	1150	>25	Structured shower
	15.0	0	50	970	—		
18	5.2	25	0	1280	~ 500	10	
19	3.4	<10	<50	910	—	~ 30	Energy of accompanying particles** $\sim 10^{10}$ ev
20	13.0	20	150	5300	370	~ 30	Energy of accompanying particles** $> 10^9$ ev
21	4.0	<10	80	1200	200	?	Energy of accompanying particles** $> 10^9$ ev
22	11.0	0	50	2340	960	?	
23	2.4	0	<50	460	370	?	
24	25.0	0	0	6000	—	?	
25	10.0	15	<50	1850	—	5	
26	3.2	0	150—200	850—1300	—	6	
27	15.0	12	50—100	4000	1300	15	
28	22.5	<10	50—100	7600	—	>30	Structured showers
	46.0	<10	$\leqslant 50$	18000	—		
29	1.6	18	150	400	450—600	1	
30	2.5±0.2	13	180	430	~ 400	—	
31	2.0	25	0	220	365	1	
32	10.0	10	125	3500	—	~ 15	Energy of accompanying particles** $\sim 2 \times 10^9$ ev

*The number of accompanying particles is given without the generating particle.

**The energy of the accompanying particles was estimated by means of data from the first row of ionization chambers.

In six cases there were no accompanying charged particles; in one of these cases the energy was about 10^{12} ev.

5. DISCUSSION OF RESULTS

An analysis of the results collected in the table and of the nuclear-cascade curves (of which examples are given in Fig. 3) leads to a number of conclusions concerning the properties, and interactions with matter, of nuclear-active particles with $10^{10}-10^{12}$ ev.

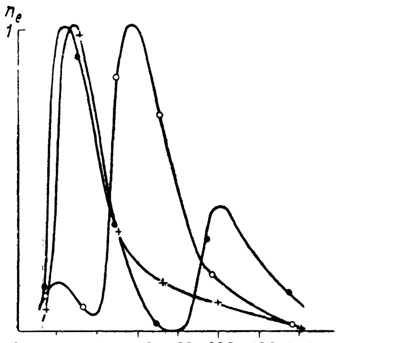

FIG. 3. Examples of nuclear-cascade curves. The vertical axis gives the number of electrons in arbitrary units (normalized to the maximum); the horizontal axis represents absorber thickness. + – nuclear-cascade curve in first group, ● and o – nuclear-cascade curves in second group.

1. Interaction Cross Section

Until recently the cross section for interactions between high-energy particles and nuclei could not be measured because of the low intensity of cosmic-ray particles with $\geq 10^{11}$ ev as well as methodological difficulties. The greatest progress was made by Williams, who measured the cross section for the interaction between iron and ~ 50-Bev nucleons.[5]

Our apparatus can determine the cross section for interactions between nuclei and nuclear-active particles above $5\times 10^{10}-10^{11}$ ev. We can record any nuclear interaction in which more than $3-5\%$ of the primary-particle energy is transferred to the soft component (at $\sim 10^{11}$ ev).

We determined the interaction mean free path of nuclear-active particles (principally nucleons) in iron, observing the distribution of cascade origins as a function of absorber thickness. The number of interactions occurring below a layer of thickness x is given by

$$N = N_0 \exp(-x/L),$$

where L is the interaction mean free path. Figure 4 is a semi-logarithmic plot of the number of interactions occurring below x thickness as a function of x.

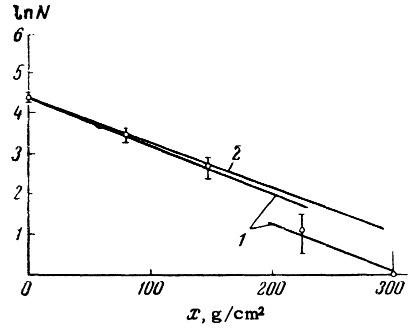

FIG. 4. Number of interactions occurring below thickness x of iron absorber as a function of x: 1 – direct experimental data without corrections, 2 – after corrections for neutrons.

The experimental results require some comment. The placing of telescopic counters under a thick layer of matter introduces discrimination into the observed events. As already mentioned, $\sim 80\%$ of all nuclear-active particles are accompanied by soft electrons as they enter the apparatus. These electrons trigger the first row of telescopic counters. Therefore our apparatus will also register neutrons which have undergone interactions above the second row of telescopic counters. The second row of counters is not triggered when neutrons interact with nuclei below it (since the soft-electron accompaniment is absorbed in the iron) and the event is not registered. Figure 3 gives the experimental data and the results of a correction for uncounted neutrons in the lower layers. This correction was based on the hypothesis that the discontinuity of the experimental straight line 1 in Fig. 4 for $x \geq 200$ g/cm^2 resulted from the omission of primary neutrons.

For the purpose of increasing the statistical information needed to determine the cross section we also used interactions of particles with from 7×10^{10} to 3×10^{11} ev which were registered above a lower threshold (47 events). The mean free path was determined using the only nuclear interactions whose core was included in the solid angle of the apparatus. These data yielded the interaction mean free path $L = 92^{+20}_{-12}$ g/cm^2, which is close to the value corresponding to the geometric nuclear cross section $r_0 = 1.4\times 10^{-13}$ cm ($L_{geom} = 105$ g/cm^2). The interaction mean free path can sometimes be reduced when two nuclear-active particles simultaneously impinge on the apparatus close enough to form a single common core. In such cases the shower will be regarded as originating at the point where one of the particles first experiences a collision and the mean free path will be reduced. Improved statistics will hereafter make it possible to select single particles striking the apparatus unaccompanied by showers, thus excluding the possibility of reducing the mean free path in this manner. However, at $10^{11}-10^{12}$ ev we have no reason to expect the frequent appearance of very close pairs of nuclear-active particles.

2. Average Inelasticity of Interactions Between $10^{11}-10^{12}$ ev Particles and Iron Nuclei

The experimental results can be used to determine the average inelasticity $\bar{\alpha}$ of interaction between nuclear-active particles and iron nuclei. $\bar{\alpha}$ can be evaluated by analyzing the average curve of the ionization $\bar{I}(x)$ produced in iron by a particle with given energy E_0. It will be seen that the average curve is based on only the mean properties of the interaction: $\bar{\alpha}$ — the mean fraction of its energy which is lost by a primary nucleon in a single pion-producing interaction, and $\bar{\beta}/L_\pi$, where $\bar{\beta}$ is the mean fraction of the energy lost by a pion in a single interaction which produces the electron-photon component and L_π is the interaction mean free path of pions (or more precisely, of all secondary particles differing in nature from the primary particles).

We have calculated the nuclear-cascade curves for different values of the inelasticity $\bar{\alpha}$, obtaining our result for $\bar{\alpha}$ by comparing the average experimental curve with the family of calculated curves.

Our apparatus registered electrons resulting from the development of an electron-photon cascade produced by gamma quanta from π^0-meson decay. If the number of quanta with energy from ϵ to $\epsilon + d\epsilon$ resulting from π^0 decay in a layer dx is $n_\gamma(\epsilon, x)\, d\epsilon\, dx/L$, the number of electrons at depth x_0 is given by

$$dn_e = \int_0^{E_0} F(\varepsilon, x_0 - x)\, n_\gamma(\varepsilon, x)\, d\varepsilon dx / L, \qquad (2)$$

where $F(\epsilon, x_0 - x)$ is the cascade curve for a photon with energy ϵ. Since $F(\epsilon, x_0 - x)/\epsilon$ depends very slightly (logarithmically) on ϵ, we obtain

$$dn_e = \frac{dx}{L}[F(\bar{\varepsilon}, x_0 - x)/\bar{\varepsilon}] \int_0^{E_0} \varepsilon n_\gamma(\varepsilon, x)\, d\varepsilon.$$

But $\int_0^{E_0} \epsilon n_\gamma(\epsilon, x)\, d\epsilon$ is the total energy of quanta liberated in a layer dx at depth x and is equal to the combined energy E_{π^0} of π^0 mesons produced in this layer. This total energy is

$$E_{\pi^0}(x)\, dx / L = [S_n(x)\, \bar{\alpha}_{\pi^0} / L + S_\pi(x)\bar{\beta} / L_\pi]\, dx,$$

where $S_n(x)$ and $S_\pi(x)$ are the energy flux of the nucleon and pion components at depth x; α_{π^0} and $\bar{\beta}$ are the corresponding mean energy fractions transferred by π^0 mesons to nucleons and charged mesons; L_π is the meson interaction mean free path. The Total number of electrons which can be observed at depth x_0 is given by

$$n_e(x_0) = \int_0^{x_0} E_{\pi^0}(x)\, [F(\bar{\varepsilon}, x_0 - x)/\bar{\varepsilon}]\, \frac{dx}{L}. \qquad (3)$$

We must now calculate the variation with depth of the energy flux of nuclear-active particles. The thickness of the absorber is reckoned from the point where the primary particle undergoes an interaction. Using the notation $\bar{\alpha}_{\pi^0} = \bar{\alpha}/3$, we can write the following equations for the variation with depth of the energy flux (assuming that π^0 mesons receive $1/3$ of the energy transferred to all π mesons):

$$dS_n = -\bar{\alpha} S_n dx / L; \quad dS_\pi = \left(\frac{2}{3}\bar{\alpha} S_n / L - \bar{\beta} S_\pi / L_\pi\right) dx.$$

These equations are solved subject to the boundary conditions (at $x = 0$)

$$S_n = (1 - \bar{\alpha}) E_0; \quad S_{\pi^+} = 2\bar{\alpha} E_0 / 3; \quad S_{\pi^0} = \bar{\alpha} E_0 / 3.$$

The results are

$$S_n(x) = (1 - \bar{\alpha}) E_0 \exp(-\bar{\alpha} x / L).$$

$$S_\pi(x) = \frac{2}{3} \frac{\bar{\alpha} E_0}{(\bar{\alpha}/L - \bar{\beta}/L_\pi)}$$

$$\times \left\{\left(\frac{1}{L} - \frac{\bar{\beta}}{L_\pi}\right) \exp\left(-\frac{\bar{\beta} x}{L_\pi}\right) - \frac{1 - \bar{\alpha}}{L} \exp\left(-\frac{\bar{\alpha} x}{L}\right)\right\}. \qquad (4)$$

After substituting these expressions in (3) and performing a numerical integration we obtain the number of electrons $n_e(x_0)$ at different absorber levels. The following circumstances must be kept in mind in connection with the integration:

1. $F(t, \bar{\epsilon})/\bar{\epsilon}$ depends very slightly (logarithmically) on $\bar{\epsilon}$. We have therefore neglected the variation with depth of the mean gamma quantum. As the cascade curve we used the curve for photons with $\epsilon = 4.5 \times 10^9$ ev which was obtained in reference 4.

2. β/L_π can be determined experimentally. A computation shows that the average curve $\bar{I}(x) \sim \bar{n}_e(x)$ depends only on the average properties of $\bar{\alpha}$ and $\bar{\beta}/L$. $\bar{\beta}/L$ can be determined from the experimental curve

$$\bar{\beta} / L_\pi = - d\bar{I}(x) / \bar{I}(x)\, dx \text{ for } x \gg L.$$

Assuming $\bar{\beta}/L = 1/3\, L$, which is our experimental result, we are left with only one unknown parameter, which can be determined by comparing the average curve with the calculations.

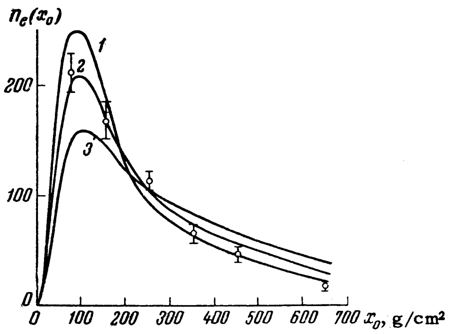

FIG. 5. Comparison of experimental results with the computed average nuclear-cascade curve: 1) $\bar{\alpha} = 1.0$, 2) $\bar{\alpha} = 0.75$, 3) $\bar{\alpha} = 0.5$

Figure 5 represents the calculations for different energy fractions transferred to pions. The experimental data shown here were converted to values for $E_0 = 10^{11}$ ev, which was used in the calulations.

To determine the average experimental curve, which our apparatus would give automatically if all interactions began at the same depth and pertained to the same primary particle energy, we proceeded as follows. All nuclear-cascade curves for $E_0 \geq 10^{11}$ ev were areally normalized to the same energy $E_0 = 10^{11}$ ev. (This reflects the assumption that the shape of the average nuclear-cascade curve is independent of E_0, at least in the range $10^{11} - 10^{12}$ ev.) Following the normalization the starting points of all experimental curves were superposed and the ordinates were added. The resulting average curve $n_e(x)$ corresponds to the assumptions used in the calculation.

The experimental result is in best agreement with an energy fraction $\overline{\alpha}$ from 0.75 to 1 and, apparently, $\overline{\alpha} > 0.5$. The inadequate statistical accuracy of our results prevents greater certainty. Under great thicknesses of matter an appreciable fraction of the energy may possibly be expended for the production of strongly ionizing particles which are not registered by our apparatus. In that event the averaged experimental curve at great depths will be steeper, thus simulating an increase of the energy loss fraction.

Some investigators[6] have noted the interesting fact that interactions between high-energy nucleons ($\sim 10^{10}$ ev and higher) and light nuclei are accompanied by low fractional energy losses. We have found that at $E_0 > 10^{11}$ ev interactions with iron nuclei are accompanied by a high degree of inelasticity. We expect that in the near future our apparatus will supply us with direct data on the relation between the inelasticity and the atomic weight of the target nucleus.

6. FLUCTUATIONS OF THE ENERGY TRANSFERRED TO π^0 MESONS

Our technique enables us in principle to determine the fraction of energy α_{π^0} transferred to π^0 mesons by nucleons in each individual collision of a nucleon with a nucleus, and thus to study the fluctuations in the transfer of energy to π^0 mesons.

In determining α_{π^0} we assumed that the principal contribution to ionization in the first few rows of ionization chambers comes from electrons arising from π^0 mesons produced in the first event. By measuring the area under the initial part of the ionization curve (which is most instances resembles the electron-photon cascade curve) we can calculate the energy transferred to π^0 mesons in the first event. At the same time we must take into account the fraction of electrons resulting from secondary nuclear interactions in the first few layers.

In the case of the first group of nuclear-cascade curves (Fig. 3) the ionization contribution of secondary interactions can be calculated quite accurately since these interactions are entirely responsible for the gradually descending part of each curve. This part can be extrapolated to the point of the first interaction by using the calculation in the preceeding section, thus giving the contribution of secondary nuclear collisions.

In determining α_{π^0} for curves of the second group difficulties arise when the second maximum is close to the first. In such cases the contribution of secondary interactions in each individual event was taken to be the average for this group; this occurred in $1/3$ of all instances. α_{π^0} could be determined more reliably when the maxima were sufficiently separated. Figure 6 shows the distribution of values of α_{π^0} in 29 interactions which were obtained by the described procedure. From this histogram it appears that the average energy transferred to π^0 mesons is $\sim 0.4 \pm 0.1$ of the primary particle energy, which is close to the most probable value of α_{π^0}. The distribution may be distorted because some of the maxima of the secondary and primary interactions are unresolved. This increases the fraction of the area

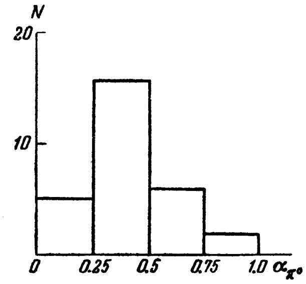

FIG. 6. Fraction of primary-particle energy transferred to π^0 mesons. N represents the number of events.

under the initial part of the nuclear-cascade curve and raises the value of α_{π^0}. Therefore the distribution shown in Fig. 6 is the distribution of fluctuations in the transfer of energy to π^0 mesons on a segment of the particle track which is $\sim 1/3$ to $1/2$ of the nuclear-component range. This distribution apparently does not differ strongly from that of α_{π^0} in a single event. The difference consists in an increased number of events with large energy loss (due to the aforementioned effect) and a small reduction of the number with low energy loss ($\alpha_{\pi^0} < 6.25$). The latter reduction results from the fact that some events with low energy loss may occur close to secondary interactions with large energy transfer which mask the former events. The corresponding correction is easily estimated to be not more than 5% of all instances (30% of all transfers of small amounts of energy).

7. ABSORPTION OF ENERGY FLUX OF NUCLEAR-ACTIVE PARTICLES UNDER GREAT THICKNESSES OF IRON

The ionization produced by the entire spectrum of primary nuclear-active particles at depth x_0 can be represented by

$$I(x_0) \sim \int_0^{x_0} \frac{dx}{L} \exp(-x/L)\, n_e(x_0 - x,\ E_0) \frac{dN}{dE_0},$$

where $n_e(x_0 - x)$ is given by (3). Since the range of the electron-photon component is smaller than that of the nuclear-active component the two components will be in equilibrium at great depths. The number of electrons $n_e(x)$ is proportional to the energy transferred to pions in one gram of absorber material, so that when the soft component is in equilibrium with the nuclear component the variation, with depth x, of the soft-component intensity will be determined only by the variation with depth of the energy E_{π^0} transferred to π^0 mesons in one gram of absorber, i.e., in the long run, the variation with depth x of the energy flux of the nuclear component.

The ionization produced in our apparatus principally by electrons will therefore vary under large absorber thickness with the same range as the energy flux of the nuclear-active component. In sections 5 and 6 it was shown that nucleons lose a large fraction of their energy through meson production in a single event. This means that the nucleons are rapidly absorbed and that under large thicknesses of matter the nuclear-active component will consist mainly of mesons, in which case we can determine β/L_π.

To determine the experimental curve of $I(x_0)$ we added all nuclear-cascade curves, which had

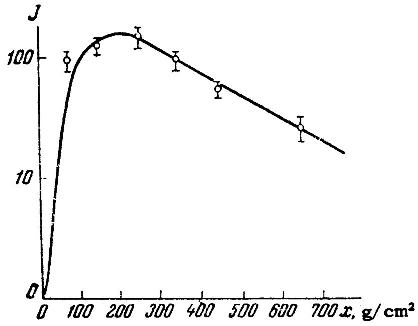

FIG. 7. Ionization I produced at different depths x of an iron absorber by nuclear-active particles with energy $E_0 > 10^{11}$ ev.

previously been reduced to the same energy through areal normalization. (This normalization led to the equating of statistical weights of the different events.) The resulting curve of $I(x_0)$ is shown in Fig. 7.

The curve is characterized by very slow reduction of the energy flux of the nuclear-active component with depth. This reduction can be described by the absorption mean free path $L_{abs} = 240\ g/cm^2$ if we neglect corrections for neutron-induced showers (at depths > 200 g/cm^2). Corrections increase the absorption mean free path to 270 g/cm^2, so that the absorption mean free path of the energy flux is about three times the nucleon interaction mean free path.

The given result is easily accounted for by the hypothesis that deep within the absorber most of the energy is concentrated in high-energy pions which in each nuclear-interaction mean free path transfer $1/3$ of their energy to π^0 mesons. The absorption mean free path is then given by L_{abs}, which is equal to $3L_{int}$ according to our experiments.

The results were obtained with the assistance of V. S. Kaftanov and graduate students Yu. G. El'kin and V. I. Lobodenko, whom the authors wish to thank.

[1] Brown, Camerini, Fowler, Heitler, King, and Powell, Phil. Mag. **40**, 862 (1949).

[2] Grigorov, Murzin, and Rapoport, J. Exptl. Theoret. Phys. (U.S.S.R.) **34**, 506 (1958), Soviet Phys. JETP **7**, 348 (1958).

[3] Grigorov, Murzin, Rapoport, and Savin, Приборы и техника эксперимента (Instruments and Measurement Engg.) No. 6, 109 (1958).

[4] I. P. Ivanenko and B. E. Samosudov, J. Exptl. Theoret. Phys. (U.S.S.R.) **35**, 1265 (1958), Soviet Phys. JETP **8**, 884 (1959).

[5] A. E. Brenner and R. Williams, Phys. Rev. **106**, 1020 (1957).

[6] Vernov, Grigorov, Zatsepin and Chudakov, Izv. Akad. Nauk SSSR Ser. Fiz. **19**, 493 (1955) (Columbia Tech. Transl. p. 445).

Translated by I. Emin
209